Available online at www.sciencedirect.com
SCIENCE DIRECT®
Journal of Catalysis 223 (2004) 191–199
JOURNAL OF CATALYSIS
www.elsevier.com/locate/jcat

The water–gas-shift reaction at short contact times

C. Wheeler, A. Jhalani, E.J. Klein, S. Tummala, and L.D. Schmidt *

Department of Chemical Engineering and Materials Science, University of Minnesota, 421 Washington Ave SE, Minneapolis, MN 55455, USA

Received 3 October 2003; revised 24 December 2003; accepted 6 January 2004

Abstract

We have examined the water–gas-shift reaction over noble metals and metals with ceria for catalyst contact times between 0.008 and 0.05 s for temperatures from 300 to 1000 °C. With reactants of CO, H_2, and H_2O at a 1/2/4 composition, the reaction approached equilibrium at these contact times for temperatures as low as 380 °C, which corresponds to a 50/1 H_2/CO ratio. All results follow the equilibrium conversion versus temperature curve at high temperatures and then the rate decreases rapidly as temperature decreases. All metals show considerable promotion upon ceria addition, with Pt/ceria showing the most promise in terms of promotion, stability, and lack of methanation activity. A simple kinetic model that assumes first-order reversible reaction in all species fits all data at all temperatures from equilibrium to low conversions. The rate is nearly independent of surface area over a wide variation of parameters, and rates indicate that mass-transfer limitations are not dominant.

Keywords: Water–gas shift; Short contact times; Pt; Ceria; Elementary-step mechanism; Noble metals; Methanation; First-order kinetics

1. Introduction

The water–gas-shift (WGS) reaction is crucial in producing H_2 from hydrocarbons, and it has been used industrially for nearly a century [1]. The conventional process for generating H_2 uses steam reforming

$$CH_4 + H_2O \rightleftharpoons CO + 3H_2 \quad \Delta H = 205.8\ \text{kJ/mol} \tag{1}$$

on Ni catalysts at ∼ 800 °C. This reaction is endothermic and reversible, so high temperatures are required for high conversions.

If pure H_2 is desired, the CO must be further reacted with H_2O to form CO_2 and an additional mole of H_2 in the water–gas-shift reaction

$$CO + H_2O \rightleftharpoons CO_2 + H_2 \quad \Delta H = -41.2\ \text{kJ/mol}. \tag{2}$$

This reaction is mildly exothermic and reversible and requires low temperatures for high equilibrium conversions. The conventional water–gas-shift catalysts which have been used in industry for nearly a century are Fe–Cr_2O_3 at ∼ 500 °C followed by Cu–ZnO at ∼ 200 °C. Both of these processes occur in packed-bed reactors with residence times of ∼ 1 s, and they attain nearly equilibrium compositions [1].

The need for H_2 for fuel cells and the hydrogen economy has caused a renewed interest in these processes because neither steam reforming nor conventional water–gas-shift is easily scaled down to smaller applications. This limits their applicability to large industrial systems and rules out their use in smaller systems such as transportation and portable power.

The research in our laboratory over the past decade has focused on understanding partial oxidation reactions at short contact times on noble metal catalysts and in this paper we examine the water–gas-shift reaction at short contact times. The partial oxidation of methane

$$CH_4 + \tfrac{1}{2}O_2 \rightarrow CO + 2H_2 \quad \Delta H = -36\ \text{kJ/mol} \tag{3}$$

can be carried out with high conversions of methane and high selectivities to CO and H_2 on Rh catalysts at contact times as short as 10^{-3} s [2,3]. This process can be run autothermally, thus eliminating the need for external heat as required in steam reforming. Partial oxidation can be easily scaled up or down by large factors for different applications, and it responds rapidly to transient operation at response times < 5 s [4].

In order to develop a compact reactor for H_2 production using a combination of partial oxidation, water–gas-shift and preferential oxidation, one needs to improve the water–gas-shift reactor or reactors to shorten the overall residence time

* Corresponding author.
E-mail address: schmidt@cems.umn.edu (L.D. Schmidt).

0021-9517/$ – see front matter
doi:10.1016/j.jcat.2004.01.002

while maintaining high conversions and assuring stability under transient operating conditions. If thermodynamic conversion can be achieved in water–gas-shift at these short contact times at temperatures $\sim 350\,^{\circ}\mathrm{C}$, then the product stream can be fed directly to a preferential oxidation reactor for further CO reduction to ppm levels. Fe and Cu are unsuitable for these applications because Fe readily forms coke in excess fuel and Cu is irreversibly deactivated if exposed to O_2 [1]. Long reactor residence times also imply long response times to startup and transient load conditions because of the high thermal mass of conventional water–gas-shift catalysts.

There has been considerable interest in noble metal catalysts to overcome these problems [5], and promoters such as ceria have been shown to increase the activity and low temperature performance of noble metals [6]. Gorte and co-workers have examined many noble metals under various conditions and have characterized their kinetics [7–9]. They examined mostly low-temperature, low-conversion situations and found that the reaction was nearly zero order in P_{CO}. There have been few published studies of high-conversion situations near reaction equilibrium which is the situation used in practical applications [5,6].

It is the intent of this paper to examine the WGS reaction at shorter times and higher temperatures to determine how kinetics change with temperature and how different flow conditions and catalyst flow patterns affect the process. We also examine kinetics of these reactions which are applicable over a wide range of temperature. In particular, we search for indications of mass-transfer and pore-diffusion limitations which indicate limits on surface area and on metal and ceria loadings.

A possible integrated short contact time H_2 generation reactor, starting with a catalytic partial oxidation reactor operating at 1100 to 900 °C followed by a water–gas-shift reactor in which temperature decreases progressively is sketched in Fig. 1a. In these experiments, we simulate this situation by examining the water–gas-shift reaction in a nearly isothermal reactor whose inlet is $H_2/CO/H_2O$. We did not use CH_4 and O_2 reactants because we also wanted to study methanation on the catalysts at these temperatures and contact times.

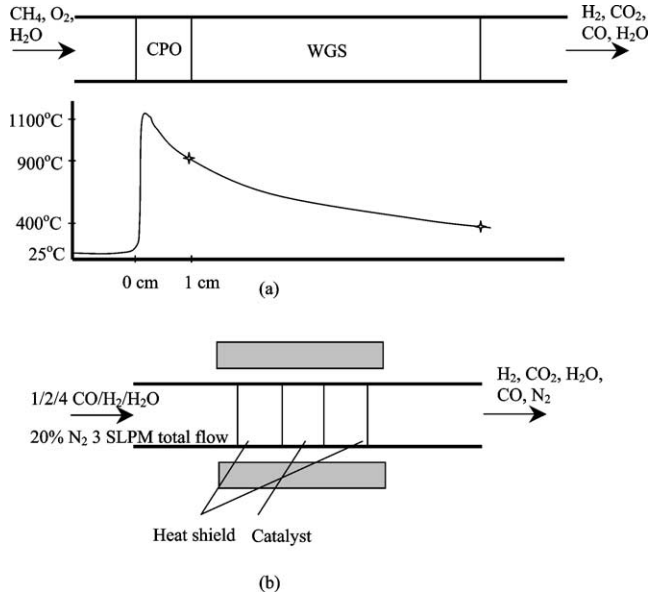

Fig. 1. (a) A possible combined catalytic partial oxidation (CPO) and water–gas-shift (WGS) reactor with a possible temperature profile along the reactor. (b) Apparatus used for water–gas-shift experiments. The reactor is a quartz tube with an inner diameter of 18 mm. Catalyst supports are either 10 mm alumina foam monoliths or alumina spheres of 1 mm diameter. Both types of support are held in place between two blank foam monoliths. Temperatures are measured at the inlet and outlet of the catalyst bed.

2. Experimental

2.1. Catalyst preparation

We used three types of catalyst supports in these experiments: (1) alumina ceramic foam monoliths containing 8% silica from Vesuvius Hi Tech Ceramics which had a nominal surface area of $\sim 1.0\ \mathrm{m}^2/\mathrm{g}$, (2) high surface area, 1-mm-diameter alumina spheres which had a nominal BET surface area of $\sim 170\ \mathrm{m}^2/\mathrm{g}$, and (3) low surface area, 1-mm-diameter alumina spheres which had a nominal BET surface area of $\sim 5\ \mathrm{m}^2/\mathrm{g}$. The behavior of various metals, both with and without ceria, was compared on the foam monolith supports, while the activity of Pt with ceria was also examined on high and low area spheres.

Monoliths had a diameter of 17 mm, 10 mm length, and a pore density of 80 pores per linear inch with a void fraction of 0.8. The monoliths were wash-coated using 3 wt% slurry of γ-aluminum oxide in distilled water followed by drying and heating at 600 °C for 6 h in a closed furnace. Wash coats were applied to increase the surface area of the monoliths. Typical wash coats were 5% by weight of monolith, for which we estimate an average alumina film thickness of 10 μm.

Metals were then coated on the supports using an aqueous solution of metal salts (H_2PtCl_6, $Rh(NO_3)_3$, $RuCl_3$, $PdCl_3$, $Ni(NO_3)_3$). The solution was dripped onto the support repeatedly, allowing the water to evaporate between applications. The monolith was then heated at 400 °C for 6 h in a closed furnace. A calculated amount of metal salt was used to ensure a 5 wt% metal loading based on the mass of the monolith.

For the catalysts combining metal with ceria, ceria was added before the metals, using a solution of $Ce(NO_3)_3$, followed by heating for 6 h at 400 °C in a closed furnace. Unless otherwise noted, a ceria loading of 5% by weight was maintained on the monolith.

For Pt and Pt/ceria we also used high and low surface area, 1-mm-diameter alumina spheres as supports. The catalyst preparation and experimental procedure for the sphere bed were analogous to those described above for monoliths. No wash coat was applied to the spheres unless otherwise

indicated. Again, the metal loading on spheres was typically 5 wt% for both Pt and ceria.

We took no special precautions to assure uniform coatings except for repeated loading and drying of the catalyst, and we regard loadings reported to be accurate to within ±20%. As will be shown and discussed later, results were not strongly sensitive to details of preparation methods, such as order of metal and ceria deposition, and heating temperature.

For some samples, areas were measured by BET analysis at various steps in catalyst preparation and use in the reactor. Total surface area did not change drastically with the addition of wash coat, ceria, or other metals. Areas varied by less than 50% overall with or without the wash coat and catalyst deposition, and before and after reaction.

2.2. Experimental procedure

All experiments were carried out in a tube furnace that could be controlled at temperatures up to 1200 °C. As depicted in Fig. 1b, the coated monolith or spheres were placed in the reactor between two blank monoliths. The monoliths were sealed into the reactor with alumina cloth. Because it was difficult to adjust the H_2O vapor flow rate, all experiments were carried out at 3 SLPM total flow rate with a feed composition of $CO/H_2/H_2O$ of 1/2/4 and 20% N_2 dilution.

Reactant gases were a 2/1 H_2/CO premixed syngas mixture and steam was added from a vaporizer. N_2 (20 mol%) was also fed for use as an internal standard for GC analysis. The syngas and N_2 flow rates were controlled using mass flow controllers. The gases were heated in a tube wrapped in heating tape prior to being fed to the reactor. Liquid water was delivered via an ISCO syringe pump, and steam was generated in a heater at approximately 700 °C. The total flow rate was set at 3 SLPM, and the molar composition of the reactant inlet stream was 22.9% H_2, 11.4% CO, 45.7% H_2O, and 20% N_2. The major cause of fluctuation in flow and temperature was intermittent condensation and evaporation of water in the system. So all experiments were conducted at a single flow rate.

The experimental procedure consisted of heating the system to 800–1000 °C such that equilibrium conversions were achieved, and then reducing the temperature in steps until negligible conversion of CO was observed. Gas samples were taken at intervals as the temperature was lowered. For each catalyst, this temperature variation procedure was carried out at least three times to verify reproducibility. Any variations in the data were largely attributed to inconsistency in the steam flow rate due to condensation and subsequent evaporation as noted previously. Blank experiments without catalytic material on the support were occasionally run to search for homogeneous reactions or reactions on impurities in the reactor. In all the cases, CO conversions without catalyst was no more than a few percent at 1000 °C.

Because the molar flow rate of reactants was held constant, the volumetric flow rate varies with temperature as predicted by the ideal gas law, and thus the contact time decreases with increasing temperature. For most experiments, temperatures were measured at the outlet of the catalyst bed. Due to the exothermicity of the reaction and possible heating and cooling of gas mixture with position, the outlet temperature was usually higher by 20 to 120 K than the inlet, depending on conversions and temperature. Reported temperatures in figures are those at the outlet of the catalyst bed. Many data points shown lie slightly above the equilibrium curve, and we attribute this discrepancy to recording conversions at the exit temperature.

Gas samples were taken through a septum at the exit of the reactor. A gas-tight syringe was used to withdraw product samples and inject it into a gas chromatograph equipped with thermal conductivity detector. Mass balances on carbon and hydrogen typically closed to within ±5%.

All experiments were repeated several times on all catalysts, with no significant differences between experiments except where noted. All catalysts were heated to at least 800 °C repeatedly during use. All catalysts were used for at least 10 h at different temperatures, and some catalysts were used for as long as 30 h. Most experiments were also repeated on several nominally identical samples with no systematic differences or deactivation noted.

3. Results

3.1. Platinum and Pt/ceria

We first show typical results from Pt and Pt/ceria on alumina foam monolith supports because they indicate the general trend for all experiments. Fig. 2 shows CO conversion versus catalyst temperature on Pt, Pt/ceria, and ceria. As

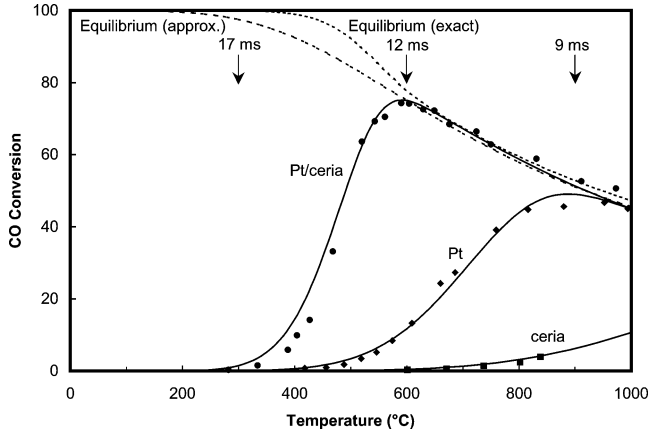

Fig. 2. CO conversions in water–gas-shift reaction on Pt, Pt/ceria, and ceria catalysts supported on an alumina foam monolith. Catalyst loading is 5% for Pt and 5% Pt/5% ceria for Pt/ceria based on the weight of the support. The upper dotted line represents equilibrium conversions for a feed composition of 1/2/4 for $CO/H_2/H_2O$ with 20% N_2 dilution. The lower dotted line represents equilibrium conversions using the empirical expression of Eq. (7). The solid lines are model fits assuming first-order reversible kinetics with respect to CO and CO_2, Eq. (10), as discussed in the text. Arrows indicate catalyst contact times at 300, 600, and 900 °C for this flow rate.

noted above, a feed mixture of $CO/H_2/H_2O$ at 1/2/4 with 20% N_2 dilution and 3 SLPM total flow was used for the experiments, and temperatures were recorded at the back face of the catalyst in the furnace.

The catalyst support for these experiments was alumina foam monolith 10 mm long. A 3 SLPM total flow corresponds to catalyst contact times from 17 ms at 300 °C, 12 ms at 600 °C, to 9 ms at 900 °C. Pt follows the equilibrium conversion down to ∼ 1000 °C and then falls rapidly so that the conversion is nearly zero by 500 °C. Pt/ceria follows the equilibrium curve down to ∼ 600 °C and falls nearly to zero by 350 °C. Ceria alone gave very low conversions at the highest temperature as shown in the figure.

The upper dashed curve in Fig. 2 shows the exact equilibrium curve calculated using Chemkin code EQUIL. The lower dashed curve in Fig. 2 shows the equilibrium calculated for this reactant composition using the expression

$$K_{eq} = K_o \exp\left(-\frac{\Delta H_R}{RT}\right) = \frac{[CO_2][H_2O]}{[CO][H_2O]}, \tag{4}$$

where

$$K_o = \frac{k_f}{k_b} \tag{5}$$

and

$$\Delta H_R = E_f - E_b. \tag{6}$$

For our reactant composition, this becomes

$$K_{eq} = \frac{X(2+X)}{(1-X)(4-X)}. \tag{7}$$

The empirical equilibrium curve in Fig. 2 deviates from the exact equilibrium curve because reactions forming CH_4 are excluded from the empirical curve expression, Eq. (4). In all subsequent figures, only the empirical equilibrium curve will be shown since it gives a lower limit on CO conversion that can be achieved in our reactor. Later in the paper we show methanation equilibrium along with methanation data for different catalysts to quantify the amount of CO that is converted to CH_4.

The reaction rate is a complex function of rate coefficients of elementary steps (16 preexponential factors and 16 activation energies for a 8-step reversible process discussed later), and the rate depends on concentrations of all reactants, products, and gas and surface intermediate species. In fitting the data, we use a very simple rate expression approximating the process as a single reversible surface reaction with rate expression

$$r'' = k_f'' P_{CO} P_{H_2O} - k_b'' P_{CO_2} P_{H_2}. \tag{8}$$

This expression assumes an elementary reaction with first-order kinetics with respect to all species. There have been many studies of kinetics of water–gas-shift reaction [7–11], and many of them report kinetics that are approximately first order in all species, either measured or assumed. For CO at lower temperatures and conversions, kinetics near zero order have been reported for ceria-supported Pd, Pt, and Rh [7,8]. For any mechanism, detailed balance requires that kinetics for this reaction approach first order in all species near thermodynamic equilibrium.

We further simplify this rate expression by assuming that H_2O and H_2 are nearly constant as CO and CO_2 change

$$r = \frac{\text{area}}{\text{volume}} r'' = k_f P_{CO} - k_b P_{CO_2}$$
$$= k_f P_{CO_O}\left(1 - X - \frac{X}{K_{eq}}\right). \tag{9}$$

The pseudo-homogeneous rate r is related to the surface reaction rate r'' by the expression $r = (\text{area}/\text{volume})r''$, where (area/volume) is the area of active catalyst per unit volume of reactor. This ratio is poorly defined for our system because the total and metal areas are not known accurately and because for ceria addition the reaction probably occurs on both metal and ceria surfaces. For this simple rate expression, the mass balance equation can be integrated assuming plug flow to give

$$X(t) = \frac{k_f}{(k_f + k_b)}\left[1 - e^{-(k_f+k_b)t}\right], \tag{10}$$

where t is the residence time in the reactor, which varies with temperature as predicted by the ideal gas law. This is the expression used to fit all data shown in this paper. The pseudo-homogeneous rate coefficients are defined as

$$k_f = \frac{\text{area}}{\text{volume}} k_f'' = \frac{\text{area}}{\text{volume}} k_{of}'' \exp\left(-\frac{E_f}{RT}\right) \tag{11}$$

so that the preexponentials k_{of} and k_{ob} have units of s^{-1}.

The curves shown along with the data points in Fig. 2 are calculated with this rate expression. A plot of $\ln X$ versus $1/T$ gave a straight line and so the activation energy was set constant at all temperatures. The forward and the backward rate constants were chosen to satisfy the equilibrium relation. The fits shown are for $k_{of} = 1.0 \times 10^6$ s^{-1} and $E_f = 80$ kJ/mol for Pt and $k_{of} = 2.5 \times 10^7$ s^{-1} and $E_f = 80$ kJ/mol for Pt/ceria. A visual inspection is sufficient to see that these curves give fits to the experimental points to within the accuracy of the data.

For all data shown in this paper, experimental points can be fit with this simple rate expression, Eq. (10). We will discuss the surprising agreement of all data on all catalysts with this expression in connection with the reaction mechanism.

3.2. Comparison of metals

In addition to Pt, we examined Rh, Ru, Pd, and Ni under identical conditions. A plot showing results for each of these metals is shown in Fig. 3. The graph shows the conversion of CO to produce CO_2. As before, the total flow rate for these experiments is 3 SLPM, resulting in a contact time of ∼ 13 ms at 500 °C.

As shown on the plot, the effectiveness of the metal catalysts follows the order Ni > Ru > Rh > Pt > Pd. The

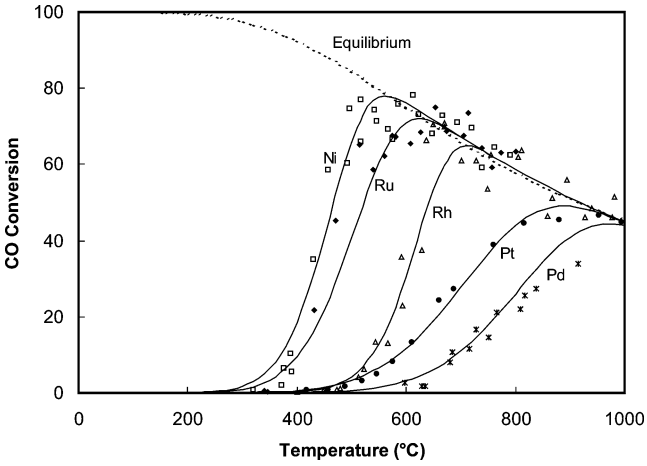

Fig. 3. CO conversions in water–gas-shift reaction on Ru, Ni, Rh, Pt, and Pd supported on alumina foam monolith. Catalyst loading is 5% based on the weight of the support. The dotted line represents equilibrium conversions for a feed composition of 1/2/4 for $CO/H_2/H_2O$ with 20% N_2 dilution using Eq. (7). The solid lines are model fits assuming first-order reversible kinetics with respect to CO and CO_2, Eq. (10).

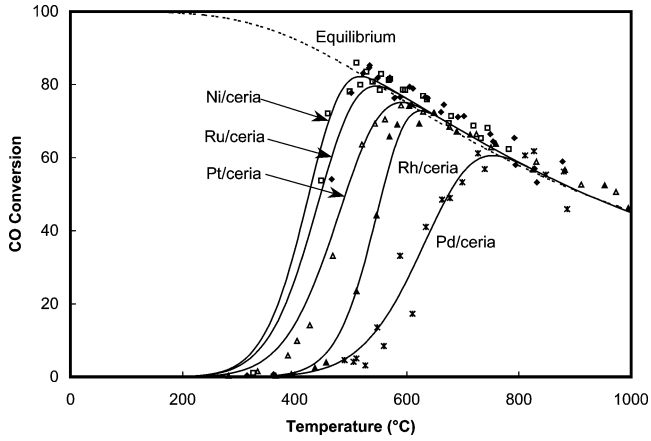

Fig. 4. CO conversions in water–gas-shift reaction on Ru/ceria, Ni/ceria, Pt/ceria, Rh/ceria, and Pd/ceria supported on alumina foam monolith. Catalyst loading is 5% metal/5% ceria based on the weight of the support. The dotted line represents equilibrium conversions for a feed composition of 1/2/4 for $CO/H_2/H_2O$ with 20% N_2 dilution using Eq. (7). The solid lines are model fits assuming first-order reversible kinetics with respect to CO and CO_2, Eq. (10).

Table 1
Preexponential factors, k_{of}, and activation energies, E_f, for metal and metal/ceria combinations

Metal or metal/ceria	k_{of} (s^{-1})	E_f (kJ/mol)	$k_{of,metal/ceria}/k_{of,metal}$
Ru	1.6×10^7	80	
Ru/ceria	5.0×10^7	80	3.12
Ni	8.0×10^7	85	
Ni/ceria	1.7×10^8	85	2.12
Rh	3.0×10^9	130	
Rh/ceria	1.5×10^{10}	130	5
Pt	1.0×10^6	80	
Pt/ceria	2.5×10^7	80	25
Pd	4.0×10^6	100	
Pd/ceria	4.0×10^7	100	10

maximum CO conversions are ∼ 80% with Ni, 75% with Ru, 70% with Rh, and 45% with Pt. The results with Pd were well below the equilibrium curve even at the highest temperature measured, ∼ 35% at 900 °C.

As discussed above, the results shown in Fig. 3 were all fit with a first-order, reversible kinetic model of Eq. (10). The constants for the model are tabulated in Table 1.

3.3. Addition of ceria to metals

We also investigated the effect of adding ceria to each of these metals, as shown in Fig. 4. The order is almost the same as that on the metals alone, Ni ≈ Ru > Pt > Rh > Pd, except that Pt and Rh are now reversed. The effect of adding ceria to the Pt catalyst, shown in Fig. 2, is the most pronounced. The equilibrium conversion is maintained down to ∼ 600 °C with Pt/ceria, versus ∼ 1000 °C with Pt alone. This results in an increase in CO conversion from 45% to about 75%. The next largest effect of adding ceria was observed with Pd. However, the activity of Pd alone was so low that even with the addition of ceria, equilibrium was achieved only down to ∼ 770 °C, yielding a CO conversion of ∼ 62%.

Although the effect of adding ceria to Ru is not as significant as that on Pt and Pd, a comparison of Figs. 3 and 4 shows that it lowers the temperature of deviation from equilibrium from 620 to 525 °C. This results in a CO conversion of ∼ 82%, and a H_2 to CO ratio approaching 16. The effects of ceria on Rh and Ni are the smallest, allowing the conversion to follow the equilibrium curve to only ∼ 50 °C lower as compared to pure metal.

The kinetic fits for metal/ceria combination, also shown in Fig. 4, agree reasonably well with the experimental data. The constants for the model are tabulated in Table 1. It should be noted that the model uses the same activation energy for metal and metal/ceria combination. The only effect of ceria is to enhance the rate of the reaction by a factor equal to the ratio of the forward rate constants for the metal/ceria and metal catalysts.

3.4. Methanation

Methane can also be formed in the reactor from the reverse steam reforming reaction, Eq. (1). Not only is CH_4 undesired in the product stream, but its formation also results in the loss of two H_2 molecules for every CH_4 molecule produced, thus lowering the H_2 to CO ratio.

Fig. 5 shows the fraction of the CO that is converted to methane, S_{CH_4}, for each metal versus temperature. The dashed line in the Fig. 5 represents the calculated equilibrium selectivity to CH_4. The order in which the metals promote methanation is Ru > Rh > Ni > Pt > Pd. Methane formation on Pt and Pd is less than 1%, while on the other metals it is large, exceeding 10% on Ru. Thus, the maximum H_2 to CO ratio on catalysts with high methanation activity

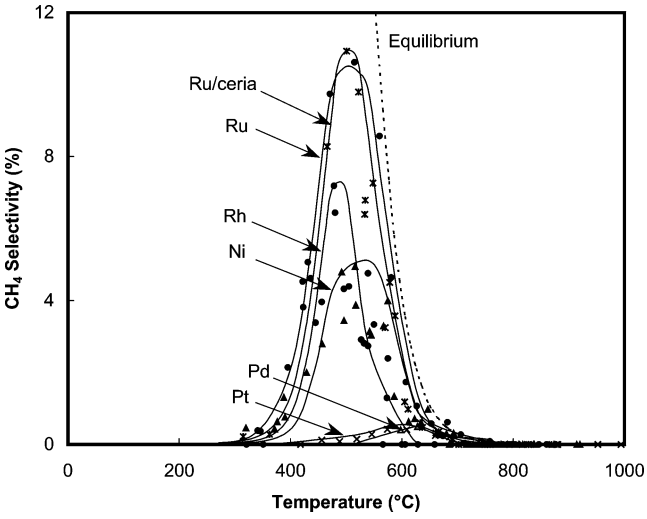

Fig. 5. Methane formation during water–gas-shift experiments on Ru, Ni, Pt, Rh, Pd, and Ru/ceria. The dashed line represents the equilibrium CH_4 selectivity calculated for a feed composition of $1/2/4$ for $CO/H_2/H_2O$ with 20% N_2 dilution.

is considerably lower than what the water–gas-shift equilibrium indicates.

We found that the addition of ceria had little effect on the amount of methane formed at a particular temperature, and results for Ru/ceria are shown in Fig. 5. One benefit of Pt/ceria catalysts was that the methanation reaction was found to be negligible at temperatures where the CO conversion was the maximum.

For most of the metals examined, no effects of carbon formation were noted from measured conversions. However, while Ni gave the highest CO conversion, it also resulted in the undesired promotion of carbon formation, which was visible both on the surface of the reactor tube downstream of the catalyst and on the foam monolith support itself after the reaction.

3.5. Comparison of supports

Three types of catalyst supports were used in this study, all alumina but covering a wide range of surface area, 1, 5, and 170 m^2/g for foam monolith, and low and high area spheres, respectively. A catalyst loading of 5 wt% Pt and 5 wt% ceria was used for these sets of experiments. Results for the various supports are compared in Fig. 6. Contact times at 400 °C are indicated in the figure for the supports. Though results differ considerably among supports, but there is little correlation of CO conversion with total area.

3.6. Comparison of residence times

To examine the effect of changing the catalyst contact time, we used a high area sphere bed of various lengths, holding the flow rate constant at 3 SLPM. Results with 5% Pt and 5% ceria loading are plotted in Fig. 7 along with model

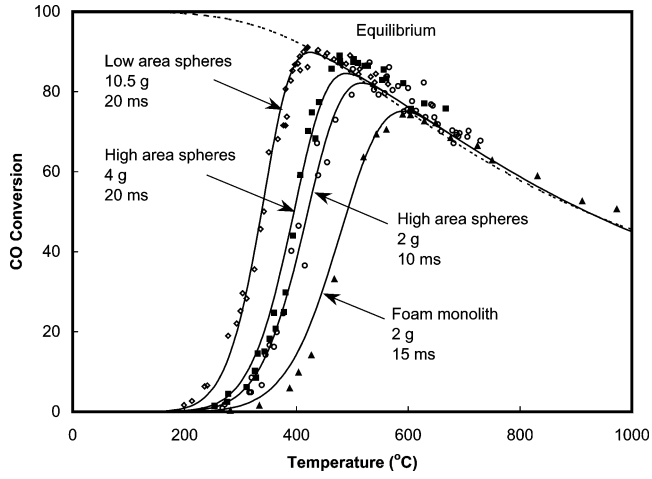

Fig. 6. The effect of catalyst support for water–gas-shift reaction on Pt/ceria. The catalyst loading in each case is 5% of the total support weight for each metal. Type and weights of catalyst support and approximate residence times at 400 °C are indicated.

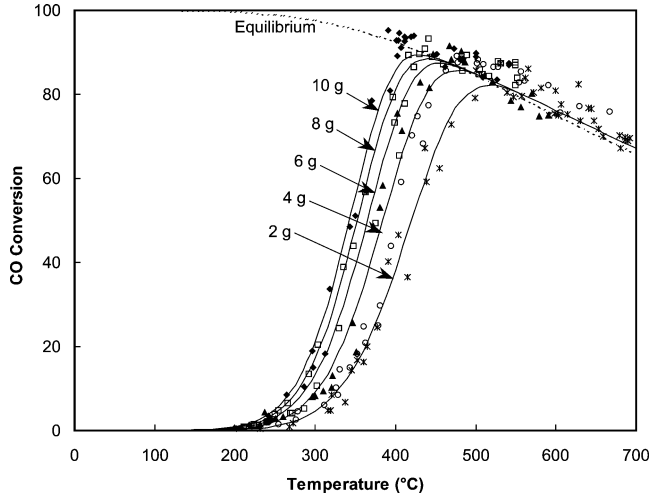

Fig. 7. The effect of increasing the catalyst amount and contact time for water–gas-shift reaction on Pt/ceria supported on high area alumina spheres. The total amount of catalyst-coated spheres is varied from 2 to 10 g, corresponding to a contact time at 400 °C of 10 to 50 ms. The solid lines are model fits assuming first-order reversible kinetics with respect to CO and CO_2 with k_{of} s proportional to catalyst amount.

fits with k_{of} s adjusted appropriately (linear dependence on catalyst amount).

A significant increase in CO conversions is achieved by lengthening the bed, as expected. The longest bed results in a CO conversion of about 95% at a temperature below 400 °C, and methane was not detectable in the product stream. Thus the highest H_2 to CO ratio attained exceeded 50 to 1.

3.7. Effect of Pt and ceria loading

To ascertain the effect of Pt and ceria loadings, experiments were performed using the low surface area alumina spheres with 5% Pt/5% ceria, 1% Pt/5% ceria, and 0.2% Pt/2% ceria catalysts. Results are plotted in Fig. 8 and show

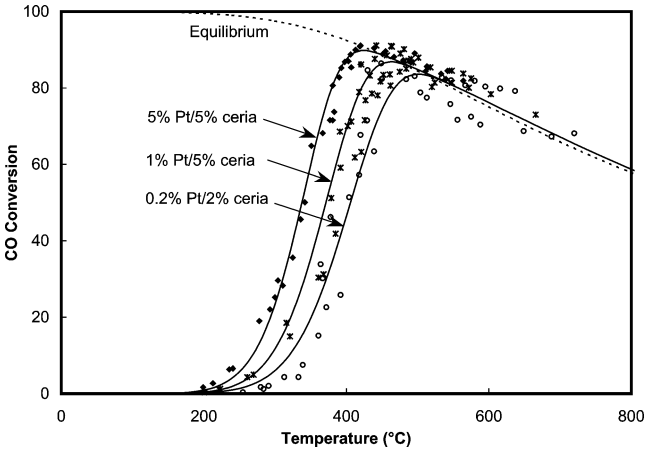

Fig. 8. The effect of different Pt and ceria loadings on CO conversions. The k_o s vary by a factor of 4.4 as Pt loading varies by a factor of 25.

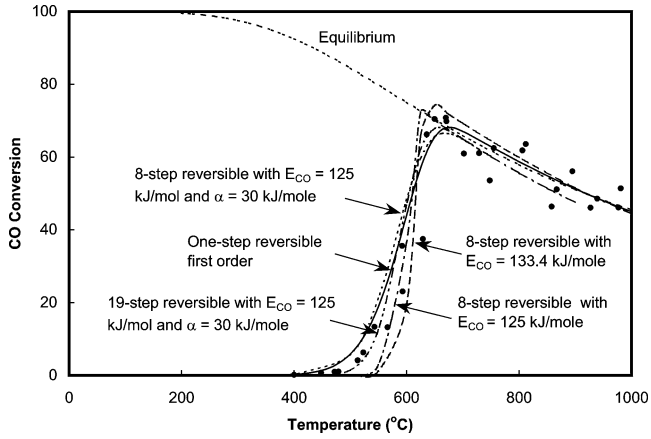

Fig. 9. Plot showing CO conversions on Rh for several models as described in the text. All models can be made to fit the experimental results to within the accuracy of the data.

that a higher loading of metal and ceria gives slightly higher CO conversions. The interesting point to be noted here is that the k_{of}'s vary by a factor of 4.4 as we move from 5% Pt/5% ceria to 0.2% Pt/2% ceria, with 5% Pt/5% ceria having a higher k_{of} than 0.2% Pt/2% ceria. Thus we observe a nonlinear dependence of k_{of} on catalyst loading as compared to a linear dependence of k_{of} on catalyst amount as discussed earlier.

4. Discussion

To summarize these results, we have measured rates of water–gas-shift reaction on five noble metal catalysts with and without ceria on monoliths and on low and high surface area alumina spheres from 300 to 1000 °C giving CO conversions from 0 to 95%. All catalysts were prepared by comparable methods and were heated to > 800 °C for at least 1 h during use. Results were highly reproducible for identically prepared samples and for repeated experiments on a given sample over 10 h. No activation or deactivation was observed except for the activation associated with the reduction of metal oxides on oxidizable metals such as Ni.

All data that we have obtained in this study can be fit to within the accuracy of the experiments with a simple reversible reaction, which assumes first-order kinetics with respect to CO and CO_2. Results on each metal can be fit with the same activation energy with and without ceria addition.

All experiments with Pt and Pt/ceria can also be fit with the same activation energy for all three supports, with and without wash coats, and for a factor of 5 variation in residence times.

In the following sections we discuss the mechanisms consistent with these experiments. We will consider detailed chemistry and simplified Langmuir–Hinshelwood kinetics, and we will discuss the effects of ceria on these reactions. Since rates appear to be nearly independent of surface areas, we will consider the effects of external mass transfer and pore diffusion through wash coats.

5. Mechanism

In this section we examine the mechanisms that may be responsible for these results and attempt to fit the results with different rate expressions. Several of these fits for water–gas shift on Rh catalysts are shown in Fig. 9.

5.1. Noble metals

The mechanism on a noble metal is assumed to consist of elementary steps such as the following sequence:

$$\begin{aligned}
&(1)\quad \mathrm{CO} + \mathrm{M} \rightleftharpoons \mathrm{CO{-}M},\\
&(2)\quad \mathrm{H_2O} + \mathrm{M} \rightleftharpoons \mathrm{H_2O{-}M},\\
&(3)\quad \mathrm{H_2O{-}M} + \mathrm{M} \rightleftharpoons \mathrm{OH{-}M} + \mathrm{H{-}M},\\
&(4)\quad \mathrm{OH{-}M} + \mathrm{M} \rightleftharpoons \mathrm{H{-}M} + \mathrm{O{-}M},\\
&(5)\quad 2\mathrm{OH{-}M} \rightleftharpoons \mathrm{H_2O{-}M} + \mathrm{O{-}M},\\
&(6)\quad \mathrm{CO{-}M} + \mathrm{O{-}M} \rightleftharpoons \mathrm{CO_2{-}M} + \mathrm{M},\\
&(7)\quad \mathrm{CO_2} + \mathrm{M} \rightleftharpoons \mathrm{CO_2{-}M},\\
&(8)\quad \mathrm{H_2} + 2\mathrm{M} \rightleftharpoons 2\mathrm{H{-}M}.
\end{aligned} \tag{12}$$

Here M is a vacant site on the noble metal surface, –M is the occupied adsorption site, steps 1, 2, 7, and 8 are adsorption and desorption steps, and steps 3, 4, 5, and 6 are surface reaction steps. We have written them all as reversible, and, assuming that all are elementary, this mechanism suggests that there are 16 rate coefficients consisting of 16 preexponential factors and 16 activation energies.

5.2. Langmuir–Hinshelwood kinetics

This is the simplest form of solution to these steps. If adsorption-desorption steps are fast and reversible and we simplify the surface reaction steps into a single step

$$\mathrm{CO{-}M} + \mathrm{H_2O{-}M} \rightleftharpoons \mathrm{CO_2{-}M} + \mathrm{H_2{-}M} \tag{13}$$

and assume it to be rate controlling, then the coverage θ_j of species j is given by the Langmuir isotherm

$$\theta_j = \frac{K_j P_j}{1 + \sum_i K_i P_i}. \tag{14}$$

Since hydrogen is dissociated, its isotherm should be proportional to $P_{H_2}^{1/2}$, but for simplicity we will leave it as P_{H_2}. The rate of reaction (13) is given by

$$r'' = k''_f \theta_{CO} \theta_{H_2O} - k''_b \theta_{CO_2} \theta_{H_2}. \tag{15}$$

With Langmuir isotherms for all species, this rate becomes

$$r'' = \frac{k''_f K_{CO} K_{H_2O} P_{CO} P_{H_2O} - k''_b K_{CO_2} K_{H_2} P_{CO_2} P_{H_2}}{(1 + K_{CO} P_{CO} + K_{H_2O} P_{H_2O} + K_{CO_2} P_{CO_2} + K_{H_2} P_{H_2})^2}. \tag{16}$$

If all the coverages are small, the denominator is unity, and the rate becomes our global expression, Eq. (8), with which we have fit all of our data. If CO is the most strongly bound compared to other species, the rate becomes

$$r'' = \frac{k''_f K_{CO} K_{H_2O} P_{CO} P_{H_2O} - k''_b K_{CO_2} K_{H_2} P_{CO_2} P_{H_2}}{(1 + K_{CO} P_{CO})^2}. \tag{17}$$

This allows the order in CO to be less than +1, and it becomes proportional to P_{CO}^{-1} as θ_{CO} approaches saturation. All of these expressions are consistent with equilibrium as long as $k''_f / k''_b = K_{eq}$, the equilibrium constant for the water–gas-shift reaction.

5.3. Detailed chemistry

For partial oxidation reactions on Rh and Pt, we and others have developed rate expressions for each of these steps [12–14], again assuming that rate coefficients for each species are independent of all coverages. All rate expressions are obtained from surface science experiments [12,15], although some of these have been adjusted to give optimum fits to a wide range of partial oxidation experiments.

We have used these rate coefficients to predict the rates of water–gas shift on Rh. We assumed a plug flow reactor and solved the set of rate equations for 7 surface species (CO, H_2O, H, O, OH, CO, and CO_2) and 4 gas phase species (CO, H_2O, CO_2, and H_2). These equations were integrated versus time up to the residence time t in the reactor. Since area/volume is not known, the time becomes an adjustable parameter in the calculation.

Fig. 9 shows results for water–gas shift on Rh along with fits to these data using four different assumptions. The first is the global expression that we have used to fit all data, Eq. (10). The second is the fit assuming detailed kinetics as described above. The temperature dependence predicted is greater than observed using an activation energy of CO, E_{CO}, of 133.4 kJ/mol. However, reducing E_{CO} to 125 kJ/mol (while simultaneously decreasing the activation energy of the CO–M + O–M reaction to maintain thermodynamic equilibrium) gives a curve that fits the experiment to within the accuracy of the data.

5.4. Coverage-dependent activation energy

A fourth fit comes from assuming that E_{CO} decreases with θ_{CO}. If we assume

$$E_{CO} = E_{CO_0} - \alpha \theta_{CO}, \tag{18}$$

we obtain good agreement between the detailed model and the experiments using $E_{CO_0} = 125$ kJ/mol and $\alpha = 30$ kJ/(mol monolayer).

5.5. Carbon model

Finally, we also fit these results using a more complete partial oxidation model that includes reactions of CH_x-adsorbed species [16]. This involves 18 reversible elementary steps where the 8-step mechanism is a subset which ignores all CH_x species.

5.6. Noble metals/ceria

In the presence of ceria, the rate is presumably greater than on the noble metals alone because H_2O can adsorb on ceria rather than being blocked by a surface saturated with CO. The mechanism with ceria might involve the steps:

$$\begin{aligned}
&(1)\quad \mathrm{CO} + \mathrm{M} \rightleftharpoons \mathrm{CO\text{–}M},\\
&(2)\quad \mathrm{H_2O} + \mathrm{Ce} \rightleftharpoons \mathrm{H_2O\text{–}Ce},\\
&(3)\quad \mathrm{H_2O\text{–}Ce} \rightleftharpoons \mathrm{O\text{–}Ce} + \mathrm{H_2},\\
&(4)\quad \mathrm{CO\text{–}M} + \mathrm{O} - \mathrm{Ce} \rightleftharpoons \mathrm{CO_2\text{–}Ce} + \mathrm{M},\\
&(5)\quad \mathrm{CO_2\text{–}Ce} \rightleftharpoons \mathrm{CO_2} + \mathrm{Ce}.
\end{aligned} \tag{19}$$

Since the overall activation energy is observed to be the same for each metal with or without ceria, this suggests that the effect of ceria is to increase rate of the reaction between adsorbed CO on the metal and O on ceria, step (4) above. If the activation energy of this step is small, the overall activation energy of the process might be unaffected, as observed.

We suggest the possibility that, even without ceria, some reaction steps might occur on the support. H_2O and CO could adsorb on alumina, similar to the steps sketched above, and reaction between O and CO could be a reaction step at high pressures and temperatures.

5.7. Preexponential factors

The adjustable parameters in all fits were the preexponential factors k_{of} and k_{ob}, whose ratio was constrained to agree with equilibrium as summarized in Table 1. Since k_o's contain an effective area/volume, these preexponentials have no simple significance since area/volume is not known. However, the only effect of ceria is to increase k_{of}'s, typically by factors of 2 to 25 on the different metals.

The most extensive experiments were on Pt and Pt/ceria. For these systems the variations in k_{of}'s were small for different supports, typically by factors less than 6. Results are

nearly independent of total surface area of the support which varied by a factor of ~ 170. Of course, the Pt surface area may not have varied by this amount because the metal particle size may compensate for substrate area variations.

6. Mass-transfer and pore-diffusion limitations

Since one is interested in minimizing contact times of reactants over the catalysts, this requires that catalyst be optimized to maximize mass-transfer and limit pore-diffusion influences.

Mass transfer of reactants to the catalyst surface and mass transfer of products from the surface are described by noting that at steady state the mass flux from a flowing channel to the catalyst surface must be equal to the reaction at an external surface if mass transfer is rate controlling [17],

$$\text{flux of reactant } A = k_{\mathrm{m}A}(C_{\mathrm{A}} - C_{\mathrm{As}}) = \text{rate of reaction of } A = r'' = k'' C_{\mathrm{As}}, \tag{20}$$

where $k_{\mathrm{m}A}$ is the mass-transfer coefficient, C_{A} and C_{As} are the concentrations in the flowing stream and at the catalyst surface, respectively, and k'' is the surface reaction rate coefficient. In this expression we assume first-order, irreversible reaction in the reactant A, from which the reaction rate versus the reactant concentration in the flowing stream is given by

$$r'' = k'' C_{\mathrm{A}} \tag{21}$$

if reaction limited, and

$$r'' = k_{\mathrm{m}A} C_{\mathrm{A}} \tag{22}$$

if mass-transfer limited.

If the catalyst is a porous support layer impregnated with the catalyst, the reactant concentration will decline through the catalyst pore because of diffusion resistance, and the consequent effect on rate is described by multiplying the rate at the external surface of the porous catalyst by an effectiveness factor $\eta(\phi)$, where ϕ is the Thiele modulus, defined as

$$\phi = \left(\frac{4k''}{d D_{\mathrm{A}}}\right)^{1/2} l, \tag{23}$$

where d is the average pore diameter, D_{A} is the diffusion coefficient of A in the porous catalyst layer, and l is the pore length.

In the limiting situation where $\phi \gg 1$, the rate is predicted to be proportional to $k''^{1/2}$ which predicts an activation energy that is $\frac{1}{2}$ of the actual reaction activation energy. Since the results are consistent with constant rate parameters at all temperatures, we conclude that there is no evidence of either external mass transfer (rate nearly independent of T) and pore-diffusion limitation (activation energy $\frac{1}{2}$ of actual value).

7. Summary

The results in this paper show that noble metal catalysts with ceria can give very high water–gas-shift activity at very short contact times. Further, these catalysts are very stable, withstanding reaction conditions above 800 °C with no detectable deactivation over many hours of operation.

These systems are very different than conventional water–gas-shift catalysts in that we use very high metal and ceria loadings and very low area catalyst supports. Therefore, these catalysts have large particle sizes initially, and they are therefore resistant to activity loss due to sintering. Results are insensitive to total surface area, although this is not correlated with evidence of either mass-transfer or pore-diffusion limitations.

The kinetics of these reactions is also remarkably simple, being consistent with an elementary reaction that is first order in all species and single activation energy for each metal with or without ceria. However, we have not tested this expression under wide ranges in partial pressures, so deviations may of course occur.

Catalysts of this type could be useful in small applications where robustness is essential and catalyst cost is not a primary concern. However, while catalyst loadings are higher than in conventional catalysts, the very short contact times required compensates for the total amount of metal required, and we have not attempted to optimize the amount of metal needed.

Acknowledgments

This research was partially supported by grants from NSF and DOE.

References

[1] M.V. Twigg, in: Catalyst Handbook, Manson, Frome, England, 1996, p. 283.
[2] D.A. Hickman, L.D. Schmidt, Science 259 (1993) 343.
[3] P.M. Witt, L.D. Schmidt, J. Catal. 163 (1996) 465.
[4] C.A. Leclerc, J.M. Redenius, L.D. Schmidt, Catal. Lett. 79 (2002) 39.
[5] A.F. Ghenciu, Curr. Opin. Solid State Mater. Sci. 6 (2002) 389.
[6] B.I. Whittington, C.J. Jiang, D.L. Trimm, Catal. Today 26 (1995) 41.
[7] T. Bunluesin, R.J. Gorte, G.W. Graham, Appl. Catal. B 15 (1998) 107.
[8] S. Hilaire, X. Wang, T. Luo, R.J. Gorte, J. Wagner, Appl. Catal. A 215 (2001) 271.
[9] X. Wang, R.J. Gorte, Appl. Catal. A 247 (2003) 157.
[10] D.C. Grenoble, M.M. Estadt, D.F. Ollis, J. Catal. 67 (1981) 90.
[11] T. Shido, Y. Iwasawa, J. Catal. 141 (1993) 71.
[12] D.A. Hickman, L.D. Schmidt, AIChE J. 39 (1993) 1164.
[13] C.T. Goralski, R.P. O'Connor, L.D. Schmidt, Chem. Eng. Sci. 55 (2000) 1357.
[14] O. Deutschmann, L.D. Schmidt, AIChE J. 44 (1998) 2465.
[15] W.R. Williams, C.M. Marks, L.D. Schmidt, J. Phys. Chem. 96 (1992) 5922.
[16] R. Schwiedernoch, S. Ticher, C. Correa, O. Deutschmann, Chem. Eng. Sci. 58 (2003) 633.
[17] L.D. Schmidt, in: The Engineering of Chemical Reactions, Oxford Univ. Press, New York, 1998, p. 283.